Ceramics International 42 (2016) 13555–13561

Contents lists available at ScienceDirect

Ceramics International

journal homepage: www.elsevier.com/locate/ceramint

Improved photoluminescence emission and gas sensor properties of ZnO thin films

D. Berger [a], A.P. de Moura [a], L.H. Oliveira [a], W.B. Bastos [a], F.A. La Porta [b,*], I.L.V. Rosa [c], M.S. Li [d], S.M. Tebcherani [e], E. Longo [a], J.A. Varela [a]

[a] UNESP, Instituto de Química, CEP 14800-900 Araraquara, SP, Brazil
[b] UTFPR, Departamento de Química, CEP 86036-370 Londrina, PR, Brazil
[c] UFSCar, Departamento de Química, CEP 13565-905 São Carlos, SP, Brazil
[d] USP, Instituto de Física de São Carlos, CEP 13560-970 São Carlos, SP, Brazil
[e] UTFPR, Departamento de Engenharia de Produção, CEP 84016-210 Ponta Grossa, PR, Brazil

ARTICLE INFO

Article history:
Received 11 March 2016
Received in revised form
17 May 2016
Accepted 23 May 2016
Available online 24 May 2016

Keywords:
ZnO
Thin films
Pressure-assisted thermal annealing
Photoluminescence properties
Gas sensor properties

ABSTRACT

In this article, we report a comparative study of the influence of pressure-assisted (1.72 MPa) versus ambient pressure thermal annealing on both ZnO thin films treated at 330 °C for 32 h. The effects of pressure on the structural, morphological, optical, and gas sensor properties of these thin films were investigated. The results show that partial preferential orientation of the wurtzite-structure ZnO thin films in the [002] or [101] planes is induced based on the thermal annealing conditions used (i.e., pressure assisted or ambient pressure). UV–vis absorption measurements revealed a negligible variation in the optical -band gap values for the both ZnO thin films. Consequently, it is deduced that the ZnO thin films exhibit different distortions of the tetrahedral [ZnO_4] clusters, corresponding to different concentrations of deep and shallow level defects in both samples. This difference induced a variation of the interface/bulk-surface, which might be responsible for the enhanced optical and gas sensor properties of the pressure-assisted thermally annealed film. Additionally, pressure-assisted thermal annealing of the ZnO films improved the H_2 sensitivity by a factor of two.

1. Introduction

Nanocrystalline zinc oxide has been extensively studied in recent years due to its widespread application in many fields of nanotechnology (e.g., photocatalysts, piezoelectricity, gas sensors, and optoelectronic devices) [1–3]. Under ambient conditions, the bulk ZnO materials preferentially crystallize in the hexagonal wurtzite-type configuration [2], unlike other members of the semiconductor II–IV family (e.g., bulk zinc sulfide that preferentially crystallizes in the cubic zinc blende-type structure) [4]. For this reason, hexagonal ZnO nanostructures are excellent subjects for theoretical and experimental studies due to their unique physical and chemical properties that are ascribed to the high surface-to-volume ratio. These features lead to enhanced optical, electrical, catalytic, and magnetic properties [5–7]. Recently, pure and doped nanostructured ZnO thin films have been developed for the detection of toxic pollutant gases, ozone gas, combustible gases, and other compounds using nanoscale devices, which is a subject of growing importance in the domestic and industrial environments [8–10].

Detection of hydrogen (H_2) has gained importance given that hydrogen is an alternative fuel source that generates clean energy and water as the main products of its combustion. In particular, H_2 can be obtained by different routes, and one of the best known is the electrolysis of water [11,12]. However, H_2 leakage is a commonly encountered issue given that H_2 is the smallest molecule and may explode at a certain concentration. For this reason, considerable effort has been expended in the structural design of new complex materials for application as gas sensors for precise detection of H_2 with high sensitivity and rapid response. Such systems are required for the development of the hydrogen energy economy, for environmental protection, and human safety [12,13]. In this context, ZnO is one of the pioneering and most promising H_2 sensing materials due to its high chemical stability and easy fabrication [14]. Furthermore, it was reported that the operating temperature of ZnO could be reduced by doping with other elements, such as Sn, Fe, Ni, Mn, Al, Cr, Ga, In, and Sb [15–20]. Most previous ZnO gas sensors operate only at high temperatures (200–

* Corresponding author.
E-mail addresses: felipe_laporta@yahoo.com.br, felipelaporta@utfpr.edu.br (F.A. La Porta).

http://dx.doi.org/10.1016/j.ceramint.2016.05.148
0272-8842/

500 °C) [21–23], or work at room temperature under ultraviolet irradiation [24,25]. Detailed and in-depth evaluation of the effect of the degree of structural order–disorder on the electronic structure and optical properties of ZnO nanostructures has been reported in previous studies [26].

It is well-established that ZnO thin films grow as n-type or p-type semiconductors due to intrinsic defects whose modulate the physical and chemical properties. In order to achieve nanoscale devices with tunable physical characteristics based on ZnO materials, a high quality crystalline n-type ZnO thin film must first be fabricated. Enhanced electrical properties can be achieved by the intrinsic electron conduction ascribed to oxygen vacancies (V_O) and interstitial zinc ions (Zn_i) that respectively act as donor and acceptor level states [26–28]. Furthermore, adsorption and desorption of oxygen molecules occurs on the ZnO surface and grain boundaries, leading to a significant increase in the ZnO conductivity [29].

In this context, high quality layers of ZnO have been grown and evaluated mainly via vapor phase techniques such as molecular beam epitaxy (MBE), metal-organic chemical vapor deposition (MOCVD), and RF-sputtering [30–32]. However, these growth or deposition methods are very expensive and are not flexible as far as growth conditions are concerned. Therefore, solution deposition techniques such as hydrothermal, dip coating, and spin coating methods have been evaluated as alternatives [9–11]. Compared to other preparation methods, the spin-coating method for deposition of ZnO films has some important advantages (i.e., simplicity and low cost of the materials and equipment) and hence has attracted considerable attention in recent years [33]. More recently, some authors have reported the effect of high pressure-assisted thermal annealing on the structural design of thin films with enhanced physical/chemical properties [34–38].

Considering the recent research trends, the focus of this study is to investigate the influence of pressure-assisted thermal annealing on the hydrogen chemisorption sensitivity as well as on the photoluminescence properties of ZnO thin films. The as-prepared ZnO thin films are analyzed by X-ray diffraction (XRD), atomic force microscopy (AFM), field emission scanning electron microscopy (FE-SEM), micro-Raman (MR) spectroscopy, ultraviolet–visible (UV–vis) spectroscopy, and by evaluation of the photoluminescence (PL) and gas sensing response of these thin films. The experimental results suggest that pressure-assisted thermal annealing enhances the physical and chemical properties of ZnO thin films.

2. Experimental procedure

ZnO thin films were prepared by spin-coating deposition of a ZnO-based polymeric precursor solution on a silicon substrate followed by thermal annealing at 330 °C for 32 h according to a documented method [39]. In the typical procedure, the viscosity of zinc citrate solution was adjusted at 20 cP and deposited onto substrates by spin-coating in a Model 4^{00}B–^{6}NPP/Lite spinner, using a speed of 4000 rpm for 15 s This procedure was sequentially performed ten times for layer-by-layer deposition, and then the films were heat-treated at 350 °C for 4 h in a tubular furnace to remove residual organic material, followed by annealing at 500 °C for 2 h using a heating rate of 2 °C/min under ambient atmosphere. Subsequently, in order to evaluate the effect of pressure on the processing of such materials, in particular, each thin films was treated as follows: (i) the thin film were annealed at 330 °C for 32 h under atmospheric pressure (denoted CF), and (ii) in an alternative process, the thin film were subjected to pressure-assisted thermal annealing (using high pressure gas of 1.72 MPa) (denoted PF) into a hermetically closed heating chamber. A heating rate of 2 °C/min was employed for both CF and PF samples.

The ZnO films were characterized by X-ray diffraction (XRD; Rigaku, DMax2500PC, Rigaku Corporation, Tokyo, Japan) at 42 kV and 120 mA and using CuKα radiation in the 2θ range of 20–60° in steps of 2°/min. The AFM technique was used to analyze the surface of the films (AFM, NanoScope V, Bruker) using tapping mode (probe type NCH, resonance frequency of 290 kHz). The morphology and thickness of the thermally annealed films were analyzed using a field emission gun scanning electron microscope (JEOL, Model 7500F, JEOL Ltd., Tokyo, Japan). The MR spectra (T-64000 Jobin-Yvon triple monochromator coupled to a CCD detector) were obtained using the 632.81 nm beam of an He − Ne laser as excita on source, with the maximum output power maintained at 8 mw.

The optical properties of the samples were analyzed by means of UV–vis reflectance spectra and PL measurements. UV–vis diffuse reflectance spectra were collected using a spectrophotometer (Varian, Cary 5 G, Agilent Technologies, Santa Clara, CA) operating in the range of 200–800 nm with a scan step of 600 nm/min, and the measurements were taken using an integrating sphere calibrated with standard Labsphere samples in the reflectance range of 0.2–99%. The PL spectra were collected using a Thermal Jarrel-Ash Monospecmonochromator and a Hamamatsu R446 photomultiplier. The 350.7 nm (3.54 eV) excitation wavelength of a krypton ion laser (Coherent Innova) was used, with a measured power of 13 mW, on both ZnO thin films. All measurements were performed at room temperature.

The gas sensing response of the samples was measured using H_2 gas as an analyte and synthetic air as the reference gas. The electrical resistance was measured by considering the precise time at which H_2 gas was turned on (adsorption) and off (desorption) at intervals of 10 min. The working temperature was fixed at 300 °C and the gas flow (H_2 and synthetic air) was 100 cm^3/min; several cycles (from 8 to 10 cycles) were performed in order to verify the reproducibility of H_2 gas chemisorption on the ZnO thin film.

3. Results and discussions

XRD patterns were acquired in order to elucidate the long-range crystalline structure and evaluate preferential orientation of the ZnO thin films based on the conditions (i.e., CF and PF) used for thermal annealing at 330 °C for 32 h. The XRD patterns of both ZnO thin films show well-defined diffraction peaks indexed to the hexagonal ZnO structure in the $P6_3mc$ space group (Joint Committee on Powder Diffraction Standards; JCPDS, card number 36-1451). However, the analysis of the positions of the diffraction peaks for both ZnO thin films, in particular, reveals that the PF thin films is slightly shifted for high angle values in comparison with the CF thin films that can be attributed to different growth conditions. Similar trends were observed in the growth of others thin films [40,41]. Notably, the CF thin film was oriented with the *c*-axis along the [002] plane, while the PF thin film presented a strong preferred orientation in the [101] plane. No additional reflections corresponding to other compounds were found in the XRD profile of either of the two thin films.

For the wurtzite structure (a=b≠c) [42], the interplanar distance of the *Miller's index* (*hkl*) plane is related to the lattice parameters *a* and *c*. For the [002] and [101] planes, the lattice parameters were $a=3.096$ Å and $c=5.363$ Å for the ZnO CF film. Pressure compresses the crystal lattice and induces a decrease of the lattice parameters; thus, $a=2.856$ Å and $c=4.947$ Å for the ZnO PF film. These results show that high pressure sintering inhibit the grain growth process of these films [43]. To gain more insights into the slightly different in the [O-Zn-O] bond lengths on the tetrahedral [ZnO_4] clusters, the unit cell volumes can be

Table 1
Crystallite size and lattice parameters (a and c) for ZnO CF and PF thin films obtained using Scherrer's equation.

ZnO thin films	Lattice parameter a (Å)	Lattice parameter c (Å)	Cell volumes $(Å)^3$
CF	3.096	5.363	44.518
PF	2.856	4.947	34.945

calculated by the lattice parameters [42], and in principle, we used here the unit cell volumes as a strategy to demonstrate this effect on the complexes clusters. The decreasing observed in the unit cell volume values for the PF film suggests a greater polarization in the tetrahedron [ZnO_4] clusters, as basic units of ZnO crystals (e.g., each Zn atom is surrounded by four O atoms at the corners of the tetrahedron), and consequently promotes different levels of the distortions on the tetrahedron [ZnO_4] clusters in the ZnO lattice. These results might suggest a shortening of the [O–Zn–O] bonds in the tetrahedron [ZnO_4] clusters of the PF thin films. The crystallite size, lattice parameters and unit cell volumes are summarized in Table 1 and are in accordance with those of ZnO thin films prepared by the spin-coating technique [44–46]. Overall, these small differences observed in the chemical bonding of the complexes clusters, in principle, may suggest possible point defects or structural distortions which have a major impact on its electronic structure, and hence may provide important hints to a rational explanation of its physical and chemical behavior at the nanoscale. These findings are in good agreement with previous theoretical studies [26].

Fig. 2 shows FE-SEM micrographs of the ZnO CF and PF thin films, illustrating the formation an irregular spherical-like of a homogeneous film roughly columnar grains and a complete coverage of the substrate. The particle size distribution of the thin film treated under ambient pressure ranged from 15 to 70 nm, whereas that of the film treated under high pressure, ranged from 4 to 22 nm. The ZnO CF film comprised spherical, irregular grains with a porous structure (see Fig. 2(a)), while the ZnO PF thin film comprised smaller columnar grains with aspect-elongated spherical structures (see Fig. 2(d)). Based on this analysis, we believe that the nucleation and growth processes of the ZnO thin films involve nuclei formation, growth, and coalescence. In particular, crystallization of the ZnO thin films is determined by the nucleation process [45,47,48]. The thin film growth process can be described as follows: in the first step, homogeneous and heterogeneous nucleation occurs simultaneously while heat is supplied. This process is accompanied by grain growth and the contact area between the particles begins to increase. However, the FE-SEM images indicate that under both pressure conditions, the mass transportation originates from the surface of the thin film and the densification process did not occur [49]. In particular, the smaller grain size in the pressure-assisted thermally annealed ZnO thin films is due to the fast nucleation. Therefore, the formation of small particles or clusters reduces the super-saturation and hence reduces the possibility of particle coalescence.

XRD patterns, as shown in Fig. 1, confirmed preferred orientation along the [002] and [101] planes for the ZnO CF and PF films, respectively. In this case, the surface energy controls the size and morphology of the grains. During the respective sintering processes, the nucleation phase facet will dominate in the obtained crystal morphology. Based on these results, we can show that the [002] facet dominates for the CF film, while the [101] facet dominates for the PF film due to the minimum surface energy. Modifications of the nucleation mechanism as well as the kinetic coefficients of the different exposed crystal facets caused by the sintering conditions could reduce the surface energy and thus

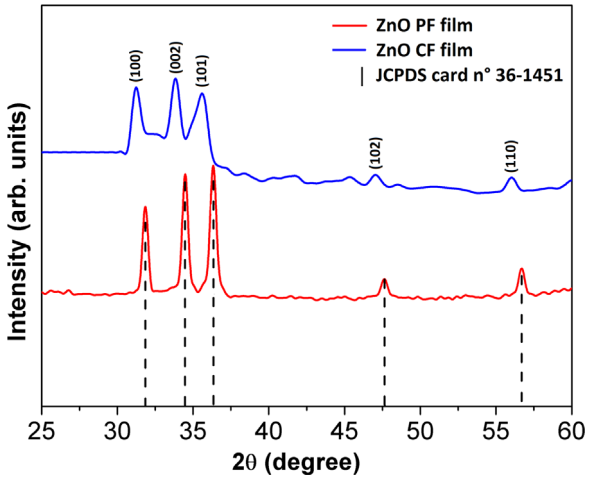

Fig. 1. XRD patterns of ZnO thin films formed under two different heat-treatment conditions: CF and PF.

govern the crystallographic orientations of these films [50]. Analysis of the cross-section of both ZnO thin films suggests that the PF film has a more active region (i.e., better contact between the nanoparticles and the substrate) than the CF film (see Fig. 2(b) and (d)).

The AFM images in Fig. 2(c) reveal that the annealing conditions used for fabrication of the ZnO CF film lead to a rather heterogeneous lateral size distribution of the grains of approximately 52.3 nm with a maximum surface height of 75 nm, while for the ZnO PF films (Fig. 2(f)), a significant reduction in the grain size distribution with an average size of about 18.2 nm and a maximum surface height of 10 nm was observed, which is in good agreement with the FE-SEM results. Note that only exposed grains were considered, thereby leading to greater precision and accuracy of the present results. Analysis of Fig. 2(c) and (f) reveals that both samples present a columnar structure and the CF film consists of spherical grains, while the BF film consists of grains with an ellipsoid-like shape, consistent with the FE-SEM results. The effective surface area (S^*) on average for these grains was estimated from the relationship between the surface area (S_A) and grain area (S_{GA}) of the spherical and elliptical models by considering the lateral size and grain height measurements using the lateral (R_L) and vertical (R_V) radius values obtained from the AFM images for an area of 500×500 nm. Fig. 3 shows the estimated S^* values obtained for both ZnO thin films. The S^* of the PF film is clearly higher than that of the CF film, and hence annealing under pressure evidently induces a decrease in the grain size of the ZnO nanoparticles. These observations suggest a large increase as a function of higher pressures, which is very interesting for gas sensing and catalytic applications.

MR spectroscopy was employed to gain insight into the short-range structural differences of the ZnO thin films (i.e., CF and PF). From group theory, the hexagonal wurtzite-type structure belongs to the space group $P6_3mc$ (C_{6v}^4) with two formula units in the primitive unit cell (Z=2) and has six optical modes, according to the irreducible representation: [51–56]

$$\Gamma_{opt} = A_1 + E_1 + 2E_2 + 2B_1 \quad (1)$$

where the A_1, E_1, and E_2 modes are Raman-active while the A_1 and E_1modes are infrared-active. The B_1 modes are silent in the Raman and infrared spectra [50–55]. The MR spectra of the ZnO thin films annealed under CF and PF conditions are presented in Fig. 4, showing five Raman active modes at 301, 430, 515, 623, and 928 cm^{-1}, which can be assigned to the $3E_{2h} - E_{2L}$, $E_{2(high)}$, A_1(LO), and E_1(LO) phonon modes respectively, and the local vibrational

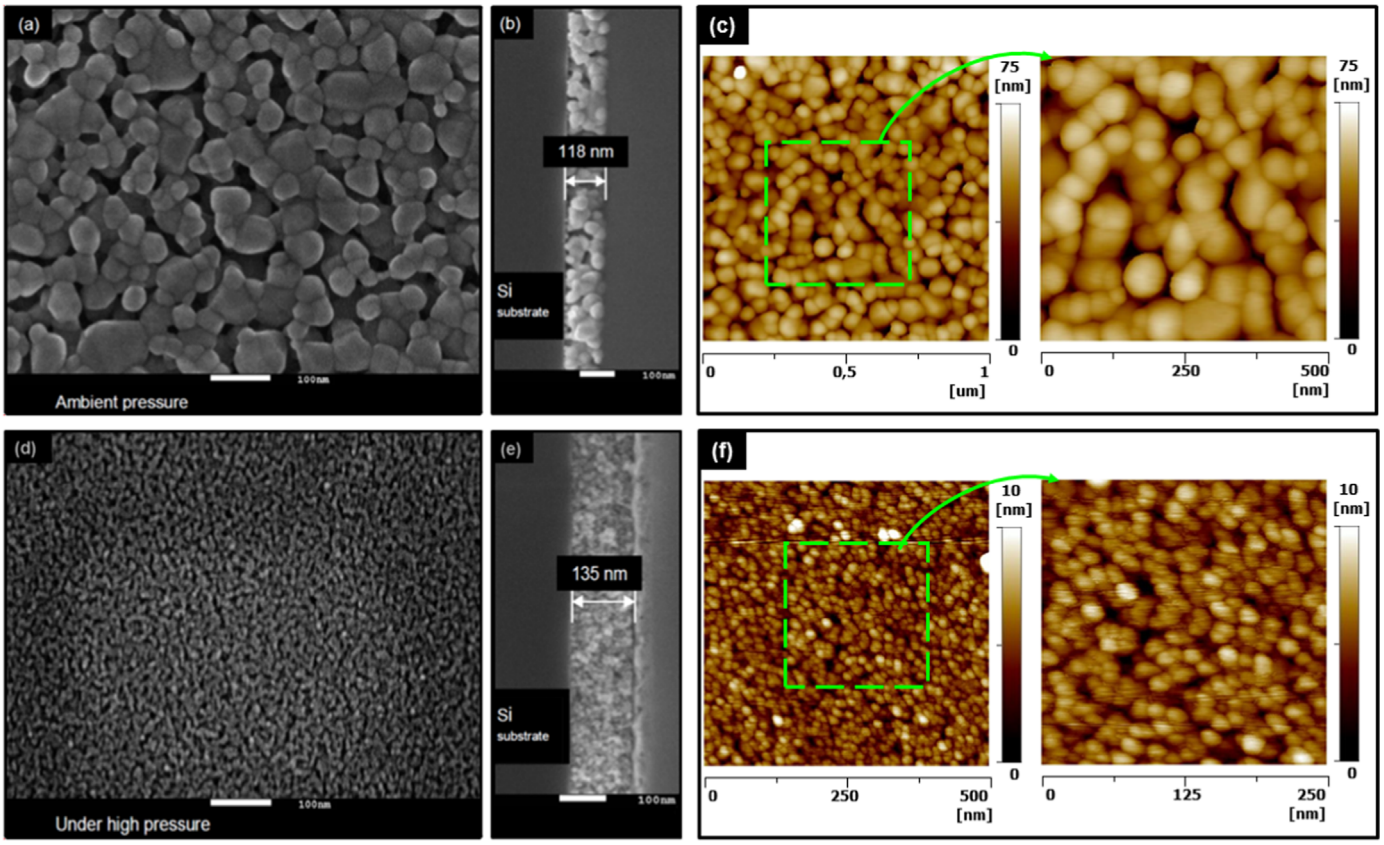

Fig. 2. FE-SEM images of ZnO films formed under CF conditions (a), cross-section (CF) (b), under PF conditions (d), cross-section (PF) (e). AFM images of ZnO CF (c) and PF thin films (f).

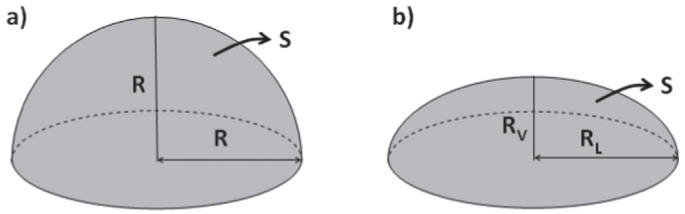

Samples	Morphology grain	R_L (nm)	R_V (nm)	S_A (nm^2)	S_{GA} (nm^2)	$S^* = S_A / S_{GA}$
CF	Spherical	26.15	26.15	351,398.13	4,296.58	81.79
PF	Ellipsoid	9.09	3.41	270,302.91	324.07	834.09

Fig. 3. Models of grain morphology for ZnO thin films: (a) spherical and (b) ellipsoid shape. Lateral radius (R_L), vertical radius (R_V), surface area (S_A), grain area (S_{GA}), and effective surface area (S^*) values for both thin films derived from AFM images of 500×500 nm area.

mode (LVM) mode located at 928 cm^{-1} can be assigned to local vibrations on the Zn and O atoms in the crystalline structure, which are consistent with previous observations [52–56]. These results suggest that the CF and PF films are structurally ordered over the short-range. Notably, narrowing of the $3E_{2h} - E_{2L}$ mode and broadening of the A_1 mode are the main effects of the thermal annealing conditions used.

On the other hand, the results indicate random growth of the columnar grains in the ZnO PF thin films, in accordance with the growth process observed in the FE-SEM and AFM images (see Fig. 2). In particular, Souissi et al. observed an increase in the intensity of the $3E_{2h} - E_{2L}$ mode for ZnO nanowires grown on (001) sapphire by metal-organic chemical vapor deposition (MOCVD) at different partial pressures. This effect was attributed to the A_1 symmetry contribution, which is favored for the randomly oriented nanowires of the ZnO films, as described previously.

To further understand the structural and electronic order-disorder effects, PL spectroscopy is a useful tool for interpretation and study of order-disorder effects in semiconductor materials over the short- and medium-range [57,58]. Fig. 4 shows the deconvoluted PL emission spectra of the ZnO thin films (i.e., CF and PF) acquired at room temperature, where the contributing spectra are

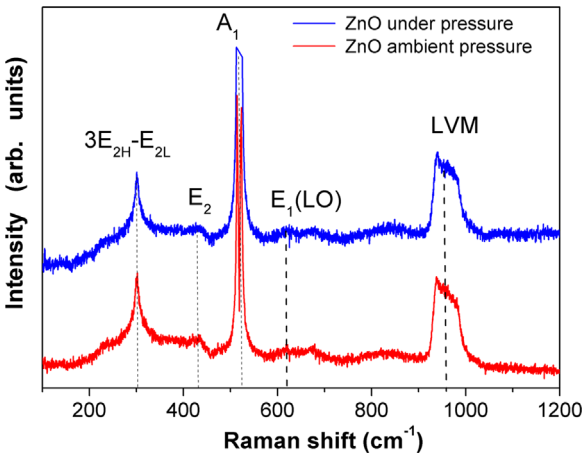

Fig. 4. Micro-Raman spectra of ZnO thin films annealed under CF and PF conditions.

Table 2
PL emission center and E_{gap} values obtained for ZnO thin films prepared by spin-coating technique treated under CF and PF conditions.

ZnO thin films	PL emission center (nm)	E_{gap} (eV)
CF	656	3.1
PF	450	3.2

typical of a multiphonon process. In addition, the UV–vis diffuse reflectance spectra were used to determine the optical band gap (E_{gap}) of these materials by the Kubelka-Munk method [4]. The maxima in the PL emission spectra and the calculated E_{gap} values for both ZnO thin films are listed in Table 2.

Analysis of Fig. 5 reveals that the broad-band in the PL emission spectrum of the ZnO CF thin film (see Fig. 5(a)) comprises four components, where the red component corresponds to the emission maximum at 650 nm. The red component represents 50.98% of the PL broad-band emission. The PL emission of the ZnO PF film is blue-shifted relative to that of the ZnO CF thin film spectrum. This shift is ascribed to the blue component (460 nm) that corresponds to 54.6% of this PL emission (Fig. 5(b)). It is noteworthy that there are several PL emission peaks for the PF film, which are intimately related with the order-disorder effects in this film. In general, the factors related to the preparation method strongly influence the environmental growth conditions, i.e., CF and PF can give rise to different degrees of structural defects that are known to modulate the physical and chemical properties of complex functional materials [26,57]. To observe PL emissions in the visible region, certain localized states must exist in the forbidden band gap, i.e., states derived from defects related to stresses and strains on the lattice (tilts), cation or anion vacancies, surface and interface states, and quantum confinement [57]. This study reveals that the formation of different types of defects (i.e., shallow and deep) in both ZnO thin films is strongly dependent on the thermal annealing conditions, and hence the deconvoluted PL emission spectra suggest that the PF film is rich in shallow level defects, while the CF film is rich in deep level defects.

In this context, for the interpretation of the PL measurements has been demonstrated that the complex cluster notation provide a better understanding of the charge transfer processes in a complex functional material with specific structural rearrangements involving electronic transitions from one cluster to another cluster [57], and they are associated with a symmetry-breaking process, i.e., to Zn displacement in the wurtzite ZnO type structure. In particular, we used the Kröger–Vink notation [59] based on the complex clusters model to explain and represent the oxygen vacancy formation (i.e., V_O^x, $V_O^\bullet$ and $V_O^{\bullet\bullet}$) in the ZnO systems, which

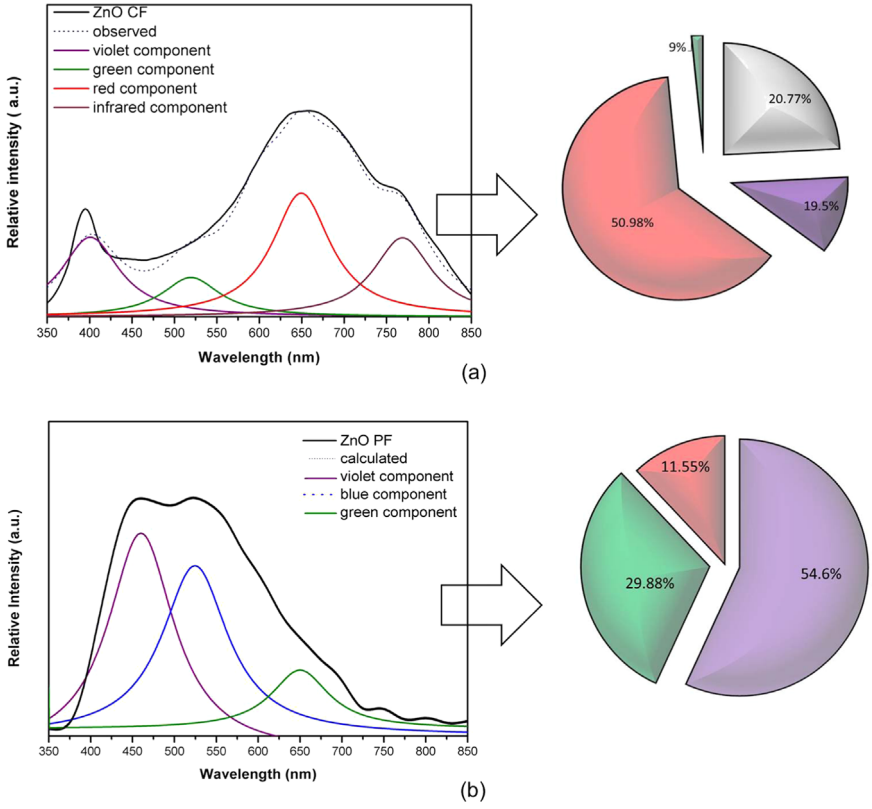

Fig. 5. Deconvoluted PL emission spectra of ZnO thin films: (a) CF and (b) PF. (For interpretation of the references to color in this figure, the reader is referred to the web version of this article.)

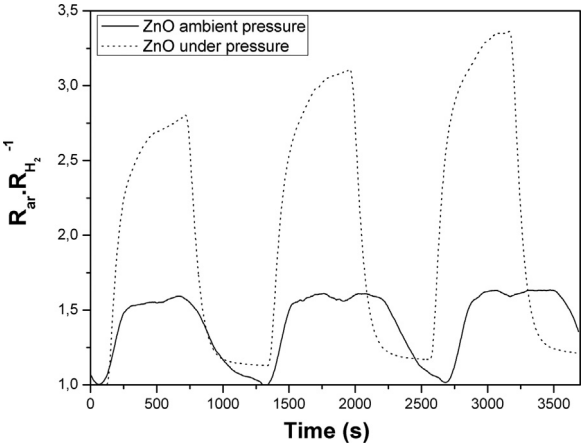

Fig. 6. Gas sensor responses of PF and CF ZnO thin films at 300 °C.

are summarized in the following equations:

$$[ZnO_3]^x–O–[ZnO_3]^x \rightarrow [ZnO_4]^x + [ZnO_3V_O^x] \quad (2)$$

$$[ZnO_4]^x + [ZnO_3V_O^x] \rightarrow [ZnO_4]' + [ZnO_3V_O^{\bullet}] \quad (3)$$

$$[ZnO_4]^x + [ZnO_3V_O^{\bullet}] \rightarrow [ZnO_4]' + [ZnO_3V_O^{\bullet\bullet}] \quad (4)$$

Here, $[ZnO_4]'$ is a donor, the $[ZnO_3 \cdot V_O^{\bullet}]$ is a donor-acceptor, and the $[ZnO_3 \cdot V_O^{\bullet\bullet}]$ is an acceptor, in according with the complex clusters model are a distorted tetrahedral cluster [26]. The present results reveal that under ambient pressure and during pressure-assisted thermal annealing, structural rearrangement of ZnO thin films may occur, thereby promoting redistribution of the intermediary states in the optical band gap (see Fig. 5 and Table 2). This fact is the main reason for the difference in the optical behavior of both ZnO thin films at the medium-range. Indeed, we believe that the great polarization observed in PF thin films are responsible for modifies the active defect sites as well as favors conditions for the stabilization of the polar surface (e.g., which are much more reactive) in the ZnO thin film. In this respect, with the specific aim to confirm these findings, we also investigated sensing of hydrogen gas for the both as-prepared ZnO thin films (see Fig. 6).

Fig. 6 shows the electrical resistance of both prepared ZnO thin films. In this case, the ZnO thin films exhibit n-type sensor behavior in response to the reducing gases. These results are consistent with other studies [60–63]. Based on these results, it is evident that the shallow defects are more important than the deep defects because the shallow defects favor the charge diffusion process and consequently inhibit carrier recombination, which is in turn favored by deep defects; this is in good agreement with the deconvoluted PL emission spectra (see Fig. 5). Therefore, the PL behavior may provide clues about the sensor properties of such films, as general trends observed for the both ZnO thin films, our results suggest that the major structural polarization observed for the PF thin films, in principle, may favors the process of the absorption and desorption of H_2 gas on ZnO thin films, leading to an improvement in the sensor behavior.

In addition to the grain size, the thickness and porosity of the ZnO thin films are other important factors for enhancing the sensing response of thin films. With smaller grain size, the specific surface area is larger and absorption and desorption of H_2 gas are facilitated. With a larger grain size, the ZnO thin film has a smaller specific surface area, causing the sensing response to be very low compared to that of the ZnO thin film treated under high pressure (see Fig. 6). The electrical resistance measurements indicated good reproducibility of the sensor response to H_2 gas. We believe that the influence of the quality of the ZnO thin films, i.e., contacts between the nanoparticles with the substrate (as discussed earlier; see Fig. 2) plays a decisive role in this behavior. However, the sensing mechanisms of both ZnO thin films under a H_2 atmosphere are still not completely clear, and further studies are required to shed light on this physical phenomenon in order to provide a deeper understanding of this dynamic process, which is beyond the scope of this report and therefore will be the target of future studies.

4. Conclusions

In summary, ZnO thin films were successfully produced via spin-coating and pressure-assisted thermal annealing. XRD, MR, FE-SEM, AFM, UV–vis, and PL measurements were employed for in-depth analysis of the structural, surface chemical composition, and optical properties of the synthesized ZnO thin films. Our results indicate that the [O-Zn-O] bonds on the tetrahedral $[ZnO_4]$ clusters is lower for the PF thin films, and therefore, suggest a strong polarization structural for such thin films. The present findings confirm that the PL of ZnO thin films is directly influenced by structural disorders that generate discrete levels in the forbidden band gap, which is critical for controlling the chemical behavior of such materials. In the light of these results the order-disorder effects induced by pressure-assisted thermal annealing is responsible, in principle, by modulating of the active defect sites as well as favors stabilization of polar surfaces in the ZnO thin films, resulting in improved PL and H_2 gas sensing properties. In short, pressure-assisted thermal annealing provides an enhancement of the physical and chemical properties of the systems studied, and offers new possibilities for creating complex functional materials and devices that can be optimized for a large number of emerging applications in the future.

Acknowledgements

The authors acknowledge the Brazilian research funding agencies FAPESP (Grant 2009/11099-2, CEPID 98/14324-0), CNPq (Grant 143451/2009-0) and FINEP (Grant 3903/06) for their financial support of this work.

References

[1] E. Rauwel, A. Galeckas, P. Rauwel, M.F. Sunding, H. Fjellvaåg, Precursor-dependent blue-green photoluminescence emission of ZnO nanoparticles, J. Phys. Chem. C 115 (2011) 25227–25233.
[2] C.F. Klingshirn, ZnO: material, physics and applications, ChemPhysChem 8 (2007) 782–803.
[3] J.-S. Tian, M.-H. Liang, Y.-T. Ho, Y.-A. Liu, L. Chang, Growth of a-plane ZnO thin films on LaAlO3(1 0 0) substrate by metal-organic chemical vapor deposition, J. Cryst. Growth 310 (2008) 777–782.
[4] F.A. La Porta, J. Andrés, M.S. Li, J.R. Sambrano, J.A. Varela, E. Longo, Zinc blende versus wurtzite ZnS nanoparticles: control of the phase and optical properties by tetrabutylammonium hydroxide, Phys. Chem. Chem. Phys. 16 (2014) 20127–20137.
[5] T. Ivanova, A. Harizanova, T. Koutzarova, B. Vertruyen, Facile deposition of ZnO:Cu films: structural and optical characterization, Mater. Sci. Semicond. Process. 30 (2015) 561–570.
[6] C.F. Klingshirn, A. Waag, A. Hoffmann, J. Geurts, Zinc Oxide: From Fundamental Properties Towards Novel Applications, Springer, Berlin, Germany, 2010.
[7] V. Kuncser, L. Miu, Size Effects in Nanostructures Basics and Applications, Springer Series in Materials Science, 2014, vol. 205.
[8] A.C. Catto, L.F. da Silva, C. Ribeiro, S. Bernardini, K. Aguir, E. Longo, V. R. Mastelaro, An easy method of preparing ozone gas sensors based on ZnO nanorods, RSC Adv. 5 (2015) 19528–19533.
[9] R. Mariappan, V. Ponnuswamy, P. Suresh, N. Ashok, P. Jayamurugan, A.

Chandra Bose, Influence of film thickness on the properties of sprayed ZnO thin films for gas sensor applications, Superlattices Microstruct. 71 (2014) 238–249.
[10] V. Musat, A.M. Rego, R. Monteiro, E. Fortunato, Microstructure and gas-sensing properties of sol–gel ZnO thin films, Thin Solid Films 516 (2008) 1512–1515.
[11] W. Lubitz, W. Tumas, Hydrogen: an overview, Chem. Rev. 107 (2007) 3900–3903.
[12] N. Monnerie, M. Roeb, A. Houaijia, C. Sattler, Coupling of wind energy and biogas with a high temperature steam electrolyser for hydrogen and methane production, Green Sustain. Chem. 5 (2014) 60–69.
[13] B. Liu, D. Cai, Y. Liu, D. Wang, L. Wang, Y. Wang, H. Li, Q. Li, T. Wang, Improved room-temperature hydrogen sensing performance of directly formed Pd/WO3 nanocomposite, Sens. Actuators B Chem. 193 (2014) 28–34.
[14] K. Vijayalakshmi, K. Karthick, D. Gopalakrishna, Influence of annealing on the structural, optical and photoluminescence properties of ZnO thin films for enhanced H2 sensing application, Ceram. Int. 39 (2013) 4749–4756.
[15] H. Shokry Hassan, A.B. Kashyout, H.M.A. Soliman, M.A. Uosif, N. Afify, Effect of reaction time and Sb doping ratios on the architecturing of ZnO nanomaterials for gas sensor applications, Appl. Surf. Sci. 277 (2013) 73–82.
[16] C.S. Prajapati, P.P. Sahay, Influence of In doping on the structural, optical and acetone sensing properties of ZnO nanoparticulate thin films, Mater. Sci. Semicond. Process. 16 (2013) 200–210.
[17] N. Vorobyeva, M. Rumyantseva, D. Filatova, E. Konstantinova, D. Grishina, A. Abakumov, S. Turner, A. Gaskov, Nanocrystalline ZnO(Ga): paramagnetic centers, surface acidity and gas sensor properties, Sens. Actuators B Chem. 182 (2013) 555–564.
[18] N.H. Al-Hardan, M.J. Abdullah, A.A. Aziz, Performance of Cr-doped ZnO for acetone sensing, Appl. Surf. Sci. 270 (2013) 480–485.
[19] F. Ahmed, N. Arshi, M.S. Anwar, R. Danish, B.H. Koo, Mn-doped ZnO nanorod gas sensor for oxygen detection, Curr. Appl. Phys. 13 (2013) S64–S68.
[20] S. Bai, T. Guo, Y. Zhao, R. Luo, D. Li, A. Chen, C.C. Liu, Mechanism enhancing gas sensing and first-principle calculations of Al-doped ZnO nanostructures, J. Mater. Chem. A 1 (2013) 11335–11342.
[21] X. Li, Y. Chang, Y. Long, Influence of Sn doping on ZnO sensing properties for ethanol and acetone, Mater. Sci. Eng. C 32 (2012) 817–821.
[22] T.T. Trinh, N.H. Tu, H.H. Le, K.Y. Ryu, K.B. Le, K. Pillai, J. Yi, Improving the ethanol sensing of ZnO nano-particle thin films—the correlation between the grain size and the sensing mechanism, Sens. Actuators B Chem. 152 (2011) 73–81.
[23] H.S. Al-Salman, M.J. Abdullah, Fabrication and characterization of ZnO thin film for hydrogen gas sensing prepared by RF-magnetron sputtering, Measurement 46 (2013) 1698–1703.
[24] J. Cui, D. Wang, T. Xie, Y. Lin, Study on photoelectric gas-sensing property and photogenerated carrier behavior of Ag–ZnO at the room temperature, Sens. Actuators B Chem. 186 (2013) 165–171.
[25] H. Ahn, Y. Wang, S. Hyun Jee, M. Park, Y.S. Yoon, D.-J. Kim, Chem. Phys. Lett. 511 (2011) 331–335.
[26] F.A. La Porta, J. Andrés, M.V.G. Vismara, C.F.O. Graeff, J.R. Sambrano, M.S. Li, J. A. Varela, E. Longo, Correlation between structural and electronic order–disorder effects and optical properties in ZnO nanocrystals, J. Mater. Chem. C. 2 (2014) 10164–10174.
[27] A. Janotti, C.G. Van de Walle, Fundamentals of zinc oxide as a semiconductor, Rep. Prog. Phys. 72 (2009) 126501.
[28] H. Kaftelen, K. Ocakoglu, R. Thomann, S. Tu, S. Weber, E. Erdem, EPR and photoluminescence spectroscopy studies on the defect structure of ZnO nanocrystals, Phys. Rev. B 86 (2012) 014113.
[29] M.F. Malek, M.H. Mamat, Z. Khusaimi, M.Z. Sahdan, M.Z. Musa, a R. Zainun, a B. Suriani, N.D.M. Sin, S.B.A. Hamid, M. Rusop, Sonicated sol–gel preparation of nanoparticulate ZnO thin films with various deposition speeds: the highly preferred c-axis (0 0 2) orientation enhances the final properties, J. Alloy. Compd. 582 (2014) 12–21.
[30] M.F. Cerqueira, T. Viseu, J. Ayres de Campos, A.G. Rolo, T. de Lacerda-Aroso, F. Oliveira, I. Bogdanovic-Radovic, E. Alves, M.I. Vasilevskiy, Raman study of insulating and conductive ZnO:(Al, Mn) thin films, Phys. Status Solidi A 212 (2015) 2345–2354.
[31] M. Opel, S. Geprägs, M. Althammer, T. Brenninger, R. Gross, Laser molecular beam epitaxy of ZnO thin films and heterostructures, J. Phys. D. Appl. Phys. 47 (2014) 034002.
[32] E. Fujimoto, M. Sumiya, T. Ohnishi, K. Watanabe, M. Lippmaa, Y. Matsumoto, H. Koinuma, Hetero-epitaxial growth of ZnO film by temperature-modulated metalorganic chemical vapor depositionv, Appl. Phys. Express 2 (2009) 045502.
[33] G. Srinivasan, N. Gopalakrishnan, Y.S. Yu, R. Kesavamoorthy, J. Kumar, Influence of post-deposition annealing on the structural and optical properties of ZnO thin films prepared by sol-gel and spin-coating method, Superlattices Microstruct. 43 (2008) 112–119.
[34] S. Cava, T. Sequinel, S.M. Tebcherani, S.R. Lazaro, S. a Pianaro, J. a Varela, Effect of temperature on glass-ceramic films prepared by impregnation of commercial float glass surfaces with oxide powders under pressure, Thin Solid Films 518 (2010) 5889–5891.
[35] S. Cava, T. Sequinel, S.M. Tebcherani, M.D. Michel, S.R. Lazaro, S. a Pianaro, Microstructure of ceramic particles infiltrated into float glass surfaces by high gas pressure impregnation, J. Alloy. Compd. 484 (2009) 877–881.
[36] S. Cava, T. Sequinel, S.M. Tebcherani, M.D. Michel, C.M. Lepienski, J.A. Varela, Nanomechanical properties of glass–ceramic films obtained by pressure impregnation of oxide powders on commercial float glass surfaces, J. Non Cryst. Solids 356 (2010) 215–219.
[37] T. Sequinel, S. Cava, J.O. Pimenta, S.A. Pianaro, S.M. Tebcherani, J.A. Varela, IR reflectance characterization of glass–ceramic films obtained by high pressure impregnation of SnO2 nanopowders on float glass, Ceram. Int. 37 (2011) 1533–1536.
[38] T. Sequinel, I.G. Garcia, S.M. Tebcherani, E.T. Kubaski, L.H. Oliveira, M. Siu Li, E. Longo, J.A. Varela, Red shift and higher photoluminescence emission of CCTO thin films undergoing pressure treatment, J. Alloy. Compd. 583 (2014) 488–491.
[39] D. Berger, E.T. Kubaski, T. Sequinel, R.M. da Silva, S.M. Tebcherani, J.A. Varela, Effect of pressure-assisted thermal annealing on the optical properties of ZnO thin films, Luminescence 28 (2013) 942–947.
[40] R.J. Gaboriaud, F. Pailloux, P. Guerin, F. Paumier, Yttrium sesquioxide, Y O, thin films deposited on Si by ion beam sputtering: microstructure and dielectric properties, Thin Solid Films 400 (2001) 106–110.
[41] B. Lacroix, F. Paumier, R.J. Gaboriaud, Crystal defects and related stress in Y2O3 thin films: origin, modeling, and consequence on the stability of the C-type structure, Phys. Rev. B 84 (2011) 014104.
[42] A. Guinier, X-rays diffraction in crystals, imperfect crystals, and amorphous bodies, W.H. Freeman, San Francisco, USA, 1963.
[43] Y. Wang, C. Yuan, L. Su, Z. Wang, J. Hao, Y. Ren, " Effect of sintering pressure on structure and magnetic properties of Zn0.99Ni0.01O bulk samples synthesized under different pressures, J. Magn. Magn. Mater. 374 (2015) 103–107.
[44] M. Smirnov, C. Baban, G.I. Rusu, Structural and optical characteristics of spin-coated ZnO thin films, Appl. Surf. Sci. 256 (2010) 2405–2408.
[45] V. Kumar, V. Kumar, S. Som, A. Yousif, N. Singh, O.M. Ntwaeaborwa, A. Kapoor, H.C. Swart, Effect of annealing on the structural, morphological and photoluminescence properties of ZnO thin films prepared by spin coating, J. Colloid Interface Sci. 428 (2014) 8–15.
[46] G. Poongodi, R.M. Kumar, R. Jayavel, Structural, optical and visible light photocatalytic properties of nanocrystalline Nd doped ZnO thin films prepared by spin coating method, Ceram. Int. 41 (2015) 4169–4175.
[47] M.W. Zhu, J.H. Xia, R.J. Hong, H. Abu-Samra, H. Huang, T. Staedler, J. Gong, C. Sun, X. Jiang, Heat-activated structural evolution of sol-gel-derived ZnO thin films, J. Cryst. Growth 310 (2008) 816–823.
[48] Y. Zhang, G. Du, X. Yang, B. Zhao, Y. Ma, T. Yang, H.C. Ong, D. Liu, S. Yang, Effect of annealing on ZnO thin films grown on (001) silicon substrate by low-pressure metalorganic chemical vapour deposition, Semicond. Sci. Technol. 19 (2004) 755–758.
[49] R.M. German, Fundam. Sinter. SCHNEIDER, S.J. Eng. Mater. Handb. Ceram. Glas., 1991, vol. 4.
[50] O. Dimitrov, D. Nesheva, V. Blaskov, I. Stambolova, S. Vassilev, Z. Levi, V. Tonchev, Gas sensitive ZnO thin films with desired (002) or (100) orientation obtained by ultrasonic spray pyrolysis, Mater. Chem. Phys. 148 (2014) 712–719.
[51] F.A. La Porta, L. Gracia, J. Andrés, J.R. Sambrano, J.A. Varela, E. Longo, A DFT study of structural and electronic properties of ZnS polymorphs and its pressure induced phase transitions, J. AM. Ceram. Soc. 97 (2014) 4011–4018.
[52] Q. Cao, S. He, Y. Deng, D. Zhu, X. Cui, G. Liu, H. Zhang, S. Yan, Y. Chen, L. Mei, Raman scattering investigations on Co-doped ZnO epitaxial films: local vibration modes and defect associated ferromagnetism, Curr. Appl. Phys. 14 (2014) 744–748.
[53] Q. Xu, X. Zhu, F. Zhang, L. Yang, W. Jiang, X. Zhou, Large-sized-mismatched group-V element doped ZnO films fabricated on silicon substrates by pulsed laser deposition, Vacuum 84 (2010) 1315–1318.
[54] W.J. Li, C.Y. Kong, H.B. Ruan, G.P. Qin, G.J. Huang, T.Y. Yang, W.W. Liang, Y. H. Zhao, X.D. Meng, P. Yu, Y.T. Cui, L. Fang, Electrical properties and Raman scattering investigation of Ag doped ZnO thin films, Solid State Commun. 152 (2012) 147–150.
[55] D.A. Guzmán-Embús, M.F. Vargas-Charry, C. Vargas-Hernández, Optical and structural properties of ZnO and ZnO:Cd particles grown by the hydrothermal method, J. Am. Ceram. Soc. 98 (2015) 1498–1505.
[56] A. Souissi, C. Sartel, A. Sayari, A. Meftah, A. Lusson, P. Galtier, V. Sallet, M. Oueslati, Zn- and O-polar surface effects on Raman mode activation in homoepitaxial ZnO thin films, Solid State Commun. 152 (2012) 794–797.
[57] E. Silva Junior, F.A. La Porta, M.S. Liu, J. Andrés, J.A. Varela, E. Longo, A relationship between structural and electronic order–disorder effects and optical properties in crystalline TiO2 nanomaterials, Dalton Trans. 44 (2015) 3159–3175.
[58] A.P. De Moura, L.H. De Oliveira, I.L.V. Rosa, C.S. Xavier, P.N. Lisboa-filho, M.S. Li, F.A. La Porta, E. Longo, J.A. Varela, Structural, optical, and magnetic properties of NiMoO4 nanorods prepared by microwave sintering, Sci. World J. 2015 (2015) 315084.
[59] F.A. Kroger, H.J. Vink, in: F. Seitz, D. Turnbull (Eds.), Solid State Physics, 3rd ed., Academic Press, New York, NY, USA, 1956, p. 307.
[60] H.V. Han, N.D. Hoa, P.V. Tong, H. Nguyen, N.V. Hieu, Single-crystal zinc oxide nanorods with nanovoids as highly sensitive NO2 nanosensors, Mater. Lett. 94 (2013) 41–43.
[61] V. Kobrinsky, E. Fradkin, V. Lumelsky, A. Rothschild, Y. Komem, Y. Lifshitz, Tunable gas sensing properties of p- and n-doped ZnO thin films, Sens. Actuator B 148 (2010) 379–387.
[62] H. Gu, Z. Wang, Y. Hu, Hydrogen gas sensors based on semiconductor oxide nanostructures, Sensors 12 (5) (2012) 5517–5550.
[63] A. Katoch, S.-W. Choi, H.W. Kim, S.S. Kim, Highly sensitive and selective H2 sensing by ZnO nanofibers and theunderlying sensing mechanism, J. Hazard. Mater. 286 (2015) 229–235.